coatings

MDPI

Article

Microstructural Changes of Al Hot-Dipped P91 Steel during High-Temperature Oxidation

Muhammad Ali Abro [1,2] and Dong Bok Lee [1,*]

[1] School of Advanced Materials Science and Engineering, Sungkyunkwan University, Suwon 16419, Korea
[2] Department of Mechanical Engineering, Mehran University of Engineering and Technology, SZAB Campus, Khairpur Mir's 66020, Pakistan; abromdali@gmail.com
* Correspondence: dlee@skku.ac.kr; Tel.: +82-31-290-7371

Academic Editor: Alessandro Lavacchi
Received: 30 December 2016; Accepted: 13 February 2017; Published: 17 February 2017

Abstract: The 9Cr-1Mo steel (ASTM P91) was hot-dip aluminized, and its microstructural changes during oxidation were studied. Before oxidation, the coating consisted of (Al-rich topcoat containing a small amount of Al_5Fe_2 and $Al_{13}Fe_4$)/($Al_{13}Fe_4$-rich, $Al_{13}Fe_4$-containing alloy layer)/(Al_5Fe_2 alloy layer containing a small amount of Al_9Cr_4 precipitates), from the surface. During oxidation at 700–900 °C for 20–100 h, Al diffused inward and the substrate elements migrated outward to broaden and soften the coating, and also to transform (high Al)-Fe intermetallics to (low Al)-Fe intermetallics. The phases in the coating progressively transformed during oxidation as follows; (Al-rich topcoat)/(Al_5Fe_2–rich, $Al_{13}Fe_4$-containing alloy layer)/(Al_5Fe_2 alloy layer)→(α-Al_2O_3 scale)/($Al_{13}Fe_4$–rich, Al_5Fe_2-containing layer)/(Al_5Fe_2 layer)/(AlFe interlayer)→(α-Al_2O_3 scale)/(AlFe–rich, Al_5Fe_2-containing layer)/(AlFe layer)/($AlFe_3$ layer))→((α-Al_2O_3, Fe_2O_3)-mixed scale)/($AlFe_3$ layer)/(Fe(Al) layer) from the surface. As the oxidation progressed, the scale changed from α-Al_2O_3 to the (α-Al_2O_3, Fe_2O_3)-mixture, which provided the necessary oxidation resistance.

Keywords: hot-dip aluminizing; P91 steel; oxidation; Al-Fe intermetallics; α-Al_2O_3

1. Introduction

The 9Cr-1Mo ferritic steel (ASTM P91) was developed to replace low-alloy ferritic steels such as 1Cr-0.5Mo (ASTM P12) and 2.25Cr-1Mo (ASTM P22). It has advantageously lower thermal expansion coefficients, better mechanical properties, and high-temperature corrosion resistance compared to low-alloy ferritic steels. It is also less expensive than austenitic stainless steels. However, the main limitation to its wide industrial application is its fast degradation at high temperatures, because scales consisting of iron oxides form due to the low Cr concentration. The critical concentration needed to form the protective Cr_2O_3 surface scale is about 10–12.5 wt % Cr for Fe-Cr alloys [1]. When 9Cr-1Mo steels oxidized at 650 °C, the scale composed of Fe_3O_4, Fe_2O_3, and $(Fe,Cr)_3O_4$ formed [2], restricting their application above 650 °C [3]. Hence, the high-temperature oxidation resistance of 9Cr-1Mo steels needs to be improved through surface modification techniques. Aluminum hot-dipping is a simple, cost-effective coating technique that could form the compact, slow growing, protective alumina scale in reaction with oxygen at high temperatures [4–15]. It also improves the surface hardness by forming Al-Fe intermetallics [5,7,9,13]. Diverse aluminized coatings have been obtained by hot-dipping carbon steels in Al [5,7,12,13] and Al-Si molten baths [5,9], 5Cr-0.5Mo steels in Al [14] and Al-Si molten baths [16], and 9Cr-1Mo steels in Al-Si [17] and Al-Si-Mg molten baths [15]. They significantly enhanced the high-temperature oxidation and corrosion resistance of the underlying steels through forming α-Al_2O_3 [5,7,9,12–14,17,18], α-Al_2O_3 + FeAl [6,15], and FeAl [16] layers. However, microstructural changes during high-temperature oxidation and the oxidation resistance of 9Cr-1Mo steels that were hot-dipped in the Al molten bath have not been adequately investigated before. The aim of this

study was to hot-dip aluminize the 9Cr-1Mo steel in order to form the Al topcoat and Al-Fe alloy layer, and examine the oxidation behavior at high temperatures. Also, the oxidation behavior of the uncoated 9Cr-1Mo steel was investigated for comparison purposes. Particular emphasis was placed on the coating thickness, coating microstructure, coating phases, and the scales that formed on the coating during oxidation at high temperatures. These characteristics vary sensitively, depending on the Al hot-dipping temperature, time, bath composition, and the composition of the substrate. The importance and influence of Al_xFe_y phases on the performance of coating is a distinct area of discussion. Our study will only be focused towards the characterization of Al hot-dipped coatings on P91 steel in order to evaluate the microstructural changes during high-temperature oxidation.

2. Materials and Methods

A P91 steel plate (80 × 30 × 3 mm^3 in size) with a nominal composition of Fe-9Cr-1Mo-0.45Mn-0.4Si-0.2V-0.08Nb-0.1C (wt %) was selected as the substrate. Both sides of the steel plate were ground to 1000 grit SiC finish, cleaned in 10 vol % HCl solution to remove the surface oxide, subjected to the liquid flux treatment with 20 vol % (KCl + AlF_3 in 4:1 weight ratio) solution, and dipped in molten Al for 5 min at 800 °C, on top of which a solid flux (KCl + NaCl + AlF_3 in 2:2:1 weight ratio) was spread to protect molten Al from oxidation. After hot dipping, the aluminized P91 steel plate was pulled out, cooled to room temperature, cleaned using 5 vol % HNO_3 solution to remove the flux on the surface, and then oxidized at 700, 800, and 900 °C for up to 100 h in air. When oxidized at 900 °C for 100 h, the uncoated steel oxidized fast, and the enhanced counterdiffusion in the coated steel made the coating and substrate somewhat ambiguous. Therefore, the time at the 900 °C condition was optimized to 20 h to show the microstructural changes of Al hot-dipped P91 steel during high-temperature oxidation. The uncoated sample was also oxidized at similar conditions for comparison purposes and in order to evaluate the diffusion mechanism using marker testing. The samples were inspected using an optical microscope (OM; Leica DM2700, Leica Microsystems, Heerbrugg, Switzerland), a field-emission scanning electron microscope (SEM; JSM-7600 F, Jeol, Tokyo, Japan) equipped with an energy dispersive spectrometer (EDS; XMAX, Oxford INCA Energy, Abingdon, UK), an electron probe microanalyzer (EPMA; Shimadzu, EPMA 1600, Kyoto, Japan), and a high-power X-ray diffractometer (HP-XRD; Bruker D8 Advance, Bruker Corporation, Karlsruhe, Germany) with Cu-Kα radiation at 40 kV and 300 mA. The microstructures of the aluminized layer and the steel substrate were etched for 10 s using Keller's reagent and Vilella's reagent, respectively. Vickers microhardness was measured using a microhardness tester (MVK-H2, Mitutoyo Corporation, Kanagawa, Japan) at a load of 100 g with an indentation time of 5 s. Hereafter, the compositions are denoted in atomic percentages (%), unless otherwise stated.

3. Results and Discussion

Figures 1 and 2 show XRD/SEM/EDS analytical results of the Al hot-dipped P91 steel. To identify the coating phases, the Al-coating was successively ground off from the surface using the abrasive paper, and X-ray analysis was performed as follows. From the surface, [Al(s), $Al_{13}Fe_4$(w)] (Figure 1a), [Al(s), $Al_{13}Fe_4$(m), Al_5Fe_2(m)] (Figure 1b), Al_5Fe_2(s) (Figure 1c), and [α-Fe(s), Al_5Fe_2(m)] (Figure 1d) phases were detected. Here, (s), (m), and (w) denote that the intensity of the diffraction patterns were strong, medium, and weak, respectively. Hot dipping formed a ~20 μm-thick topcoat (spots 1–6), ~15 μm-thick transient alloy layer (spots 7–10), and ~35 μm-thick underlying alloy layer (spots 11–19) on the steel substrate (spots 20–24) (Figure 2a). The topcoat (spots 1–6) consisted primarily of Al with a small amount of $Al_{13}Fe_4$ (in the whole topcoat) and Al_5Fe_2 (at the lower part of the topcoat). The presence of $Al_{13}Fe_4$ and the absence of Al_5Fe_2 at the upper part of the topcoat is plausible, considering the Al concentration gradient during hot dipping (Figure 1a,b). The alloy layer consisted primarily of $Al_{13}Fe_4$ (spots 7–10) and Al_5Fe_2 (spots 11–19). Al_5Fe_2 in Figure 1b–d, and α-Fe in Figure 1d belonged to the alloy layer and the substrate, respectively. White strings inside the topcoat (spots 1–6) were Al-Fe intermetallics (see Al and Fe maps of Figure 2b), which were found to be

$Al_{13}Fe_4$ and Al_5Fe_2 embedded in the Al-rich topcoat (see Figure 1a,b). While Al diffused inwards, substrate elements such as Fe and Cr diffused outwards according to the concentration gradient (Figure 2b). Orthorhombic Al_5Fe_2 had 30% vacancies along the *c*-axis, through which the counter diffusion of Al and Fe occurred rapidly [4,8,13,14,18]. Hence, the Al_5Fe_2 layer (spots 11–19) was thicker than the $Al_{13}Fe_4$ layer (spots 7–10 inside the alloy layer) [10,11]. On the other hand, in the case of low-alloyed carbon steels, the characteristic finger- or tongue-like morphology that oriented along the *c*-axis of Al_5Fe_2 generally developed at the coating/substrate interface [4–6,9,10,12,13]. Such a morphology however was not noticeable around the spots 19–20 shown in Figure 2a, because vacancies in Al_5Fe_2 were occupied more by substrate elements in the current high-alloyed Cr steel, resulting in the flattening of the coating/substrate interface and narrowing of the alloy layer. The major substrate element, Fe, diffused outward through the alloy layer into the topcoat (see the Fe map of Figure 2b), and reacted with the molten aluminum to form $Al_{13}Fe_4$ and Al_5Fe_2 strings (see spots 1–6 in Figure 2a). The enlarged image of the alloy layer revealed scattered, white particles in the alloy layer (Figure 2c). Figure 2d indicates that white particles were probably Al_9Cr_4 precipitates that could dissolve up to 32.5% Fe [19]. The counterdiffusion of Al and the substrate elements due to the concentration gradients that were generated during hot dipping resulted in the formation of the topcoat, the $Al_{13}Fe_4$ layer, and the Al_5Fe_2 layer, as shown in Figure 2e. Moving from spot 19 towards the surface, the concentration of Cr decreased from 4.9% (spot 19) to 0.1% (spot 3), whilst the other alloying elements such as Mo, Mn, Si, and V decreased from 0.5% (spot 19) to 0% (spot 3) (Figure 2e). The average composition of spots 1–2 was 99.7%Al-0.3%Fe, indicating the dissolution of Fe in Al and/or the presence of a small amount of $Al_{13}Fe_4$ in the Al-rich topcoat.

Figure 3 shows XRD/EPMA/EDS results of the Al hot-dipped P91 steel after oxidation at 700 °C for 100 h. Aluminum in the topcoat either oxidized to the α-Al_2O_3 scale or transformed to Al-Fe intermetallics through the reaction with outwardly diffusing Fe atoms, as shown in Figure 3a. Here, the α-Al_2O_3 scale formed above the ($Al_{13}Fe_4$, Al_5Fe_2)-mixed layer that originated from the Al-rich topcoat. The alloy layer that consisted of $Al_{13}Fe_4$ and Al_5Fe_2 (Figure 2a) became only Al_5Fe_2 due to the counterdiffusion of Al and the substrate elements during heating (Figure 3b). Counterdiffusion increased the coating thickness from 70 μm (spots 1–19 in Figure 2a) to 125 μm (spots 3–16 in Figure 3c). Figure 2d shows EPMA maps of the thin α-Al_2O_3 surface scale (spots 1–2 in Figure 3c), the coating that consisted primarily of Al_5Fe_2 (spots 3–16 in Figure 3c), and the steel substrate (spots 16–20 in Figure 3c). The α-Al_2O_3 oxide was susceptible to spallation owing to its mismatch of the thermal expansion coefficient with the underlying coating (see spots 1–2 in Figure 3c). Hence, the α-Al_2O_3 peak was weak in Figure 3a. Unequal mass flow and volume change due to the transformation of the topcoat and the alloy layer to $Al_{13}Fe_4$ and Al_5Fe_2 generated cracks and numerous voids in the coating [5–7,9,14,15] (Figure 3c). The loosely adherent α-Al_2O_3 scale was partially broken (see the Al map of Figure 3d). In Figure 3d, the inwardly diffusing Al diluted the concentration of Fe, Cr, and Mo in the coating. A small amount of oxygen dissolved in the coating. In Figure 3e, the α-Al_2O_3 oxide (spots 1–2) formed on the Al-Fe coating that consisted primarily of Al_5Fe_2 (spots 3–14). Around spot 3, $Al_{13}Fe_4$ coexisted with Al_5Fe_2 (see Figure 3a,e). This was plausible considering the Al concentration gradient. AlFe, which can exist in the Al concentration range of 23.3%–55%, existed at the coating/substrate interface (see spot 15 in Figure 1d). Unlike the ductile AlFe phase, $Al_{13}Fe_4$ and Al_5Fe_2 were brittle. This is another reason for the breakage and subsequent spallation of the oxide scale. The concentration of dissolved Cr decreased gradually from 4.2% (spot 14) to 0.1% (spot 1). Since Al (m.p. = 660 °C) can diffuse rapidly and readily oxidize due to its high oxygen affinity, the transformation of the topcoat and the alloy layer to the α-Al_2O_3 scale and Al-Fe intermetallics seemed to occur quickly.

The optical microstructure of Figure 3c is shown in Figure 4. The α-Al_2O_3 scale consisted of fine, round grains, because it grew slowly. Most of the coating consisted of numerous grains that elongated along the counterdiffusion direction of the Al and substrate elements. Particularly, Al_5Fe_2 grew fast perpendicular to the sample surface [4]. AlFe grains were largely square (see spot 15 in Figures 3c and 4).

The area immediately below the AlFe layer was bright, because rounding occurred during polishing due to the hardness difference between the AlFe intermetallic and the substrate.

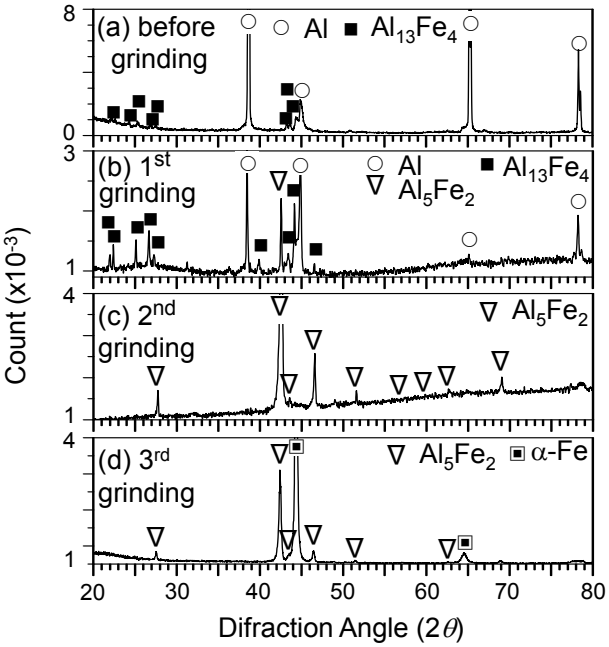

Figure 1. XRD patterns of the Al hot-dipped P91 steel: (**a**) before grinding; (**b**) after first grinding; (**c**) after second grinding; (**d**) after third grinding.

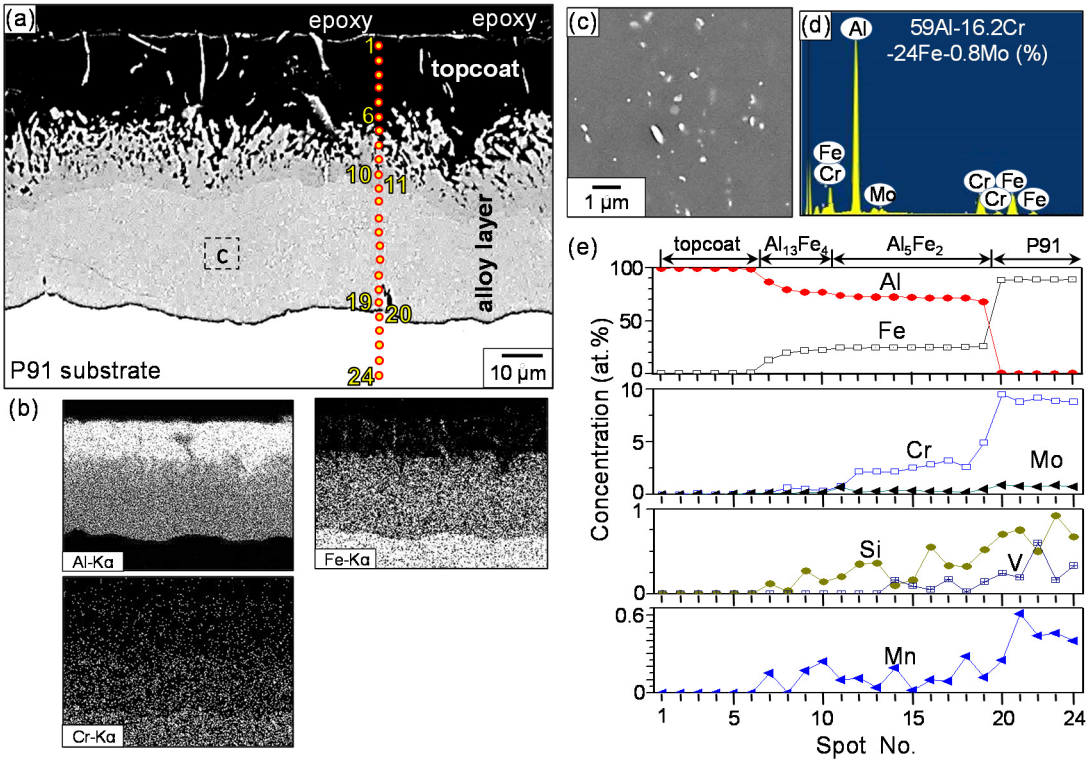

Figure 2. Al hot-dipped P91 steel. (**a**) SEM cross-sectional back-scattered electron (BSE) image (etched); (**b**) EDS maps of (**a**); (**c**) enlarged image of the rectangular area marked in (**a**); (**d**) EDS spectrum of white particles shown in (**c**); (**e**) EDS concentration profiles along the spots 1–24 marked in (**a**).

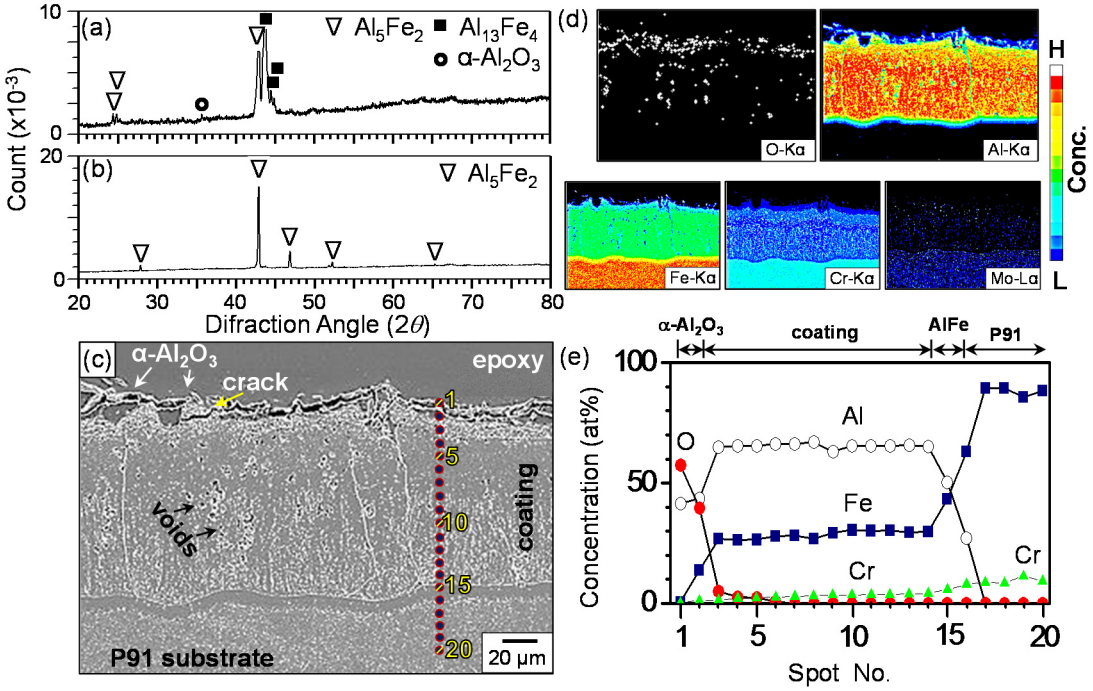

Figure 3. Al hot-dipped P91 steel after oxidation at 700 °C for 100 h. (**a**) XRD pattern before grinding; (**b**) XRD pattern after grinding off the surface; (**c**) etched electron probe microanalyzer (EPMA) cross-sectional image; (**d**) EPMA maps of (**c**); (**e**) EDS concentration profiles along spots 1–20 marked in (**c**).

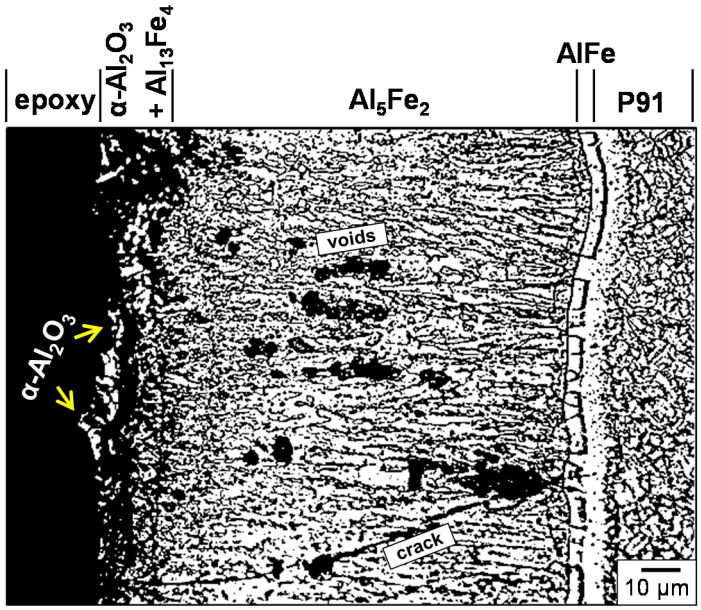

Figure 4. Optical microstructure of Al hot-dipped P91 steel after oxidation at 700 °C for 100 h (etched).

Figure 5 shows XRD/OM/EPMA results of the Al hot-dipped P91 steel after oxidation at 800 °C for 100 h. Weak α-Al_2O_3 peaks were detected in Figure 5a due to the slow growth rate and poor adherence of the α-Al_2O_3 scale. The coating just below the α-Al_2O_3 scale consisted of AlFe as the major phase and Al_5Fe_2 as the minor phase (Figure 5a). However, most of the coating consisted of AlFe (Figure 5b). In Figure 3, the coating just below the scale consisted of $Al_{13}Fe_4$ as the major phase and Al_5Fe_2 as the minor phase, while most of the coating consisted of Al_5Fe_2. Thus, it is seen

that the increment of the heating temperature from 700 to 800 °C led to the formation of Al_5Fe_2 instead of $Al_{13}Fe_4$, and AlFe instead of Al_5Fe_2 through the enhanced counterdiffusion of the Al and substrate elements. Figure 5c shows a ~4 μm-thick α-Al_2O_3 layer, ~20 μm-thick Al_5Fe_2-rich layer, ~70 μm-thick AlFe layer, ~65 μm-thick newly formed transient coating, and the substrate that consisted of equiaxed grains. Elongated Al_5Fe_2 grains shown in Figure 4 grew to coarse, columnar AlFe grains in Figure 5c. The optical image shown in Figure 5c shows the α-Al_2O_3 scale either detached or adherent, Al_5Fe_2-rich layer, AlFe layer, transient coating, and the substrate. The Kirkendall effect and the Al-Fe phase transformation generated many voids (dark spots in the coating) and some cracks (Figure 5c,d). In Figure 5e, Al diffused inwardly to the bottom of the transient coating, which was believed to consist of $AlFe_3$, because $AlFe_3$ could form between AlFe and α-Fe according to the Al-Fe binary phase diagram. In Figure 5e, the major alloying element, Cr, diffused up to the surface to dissolve in the α-Al_2O_3 layer. The second major alloying element, Mo, was denuded at the upper part of the coating owing to its small solubility in AlFe [20]. The third major alloying element, Mn, was present in the whole coating.

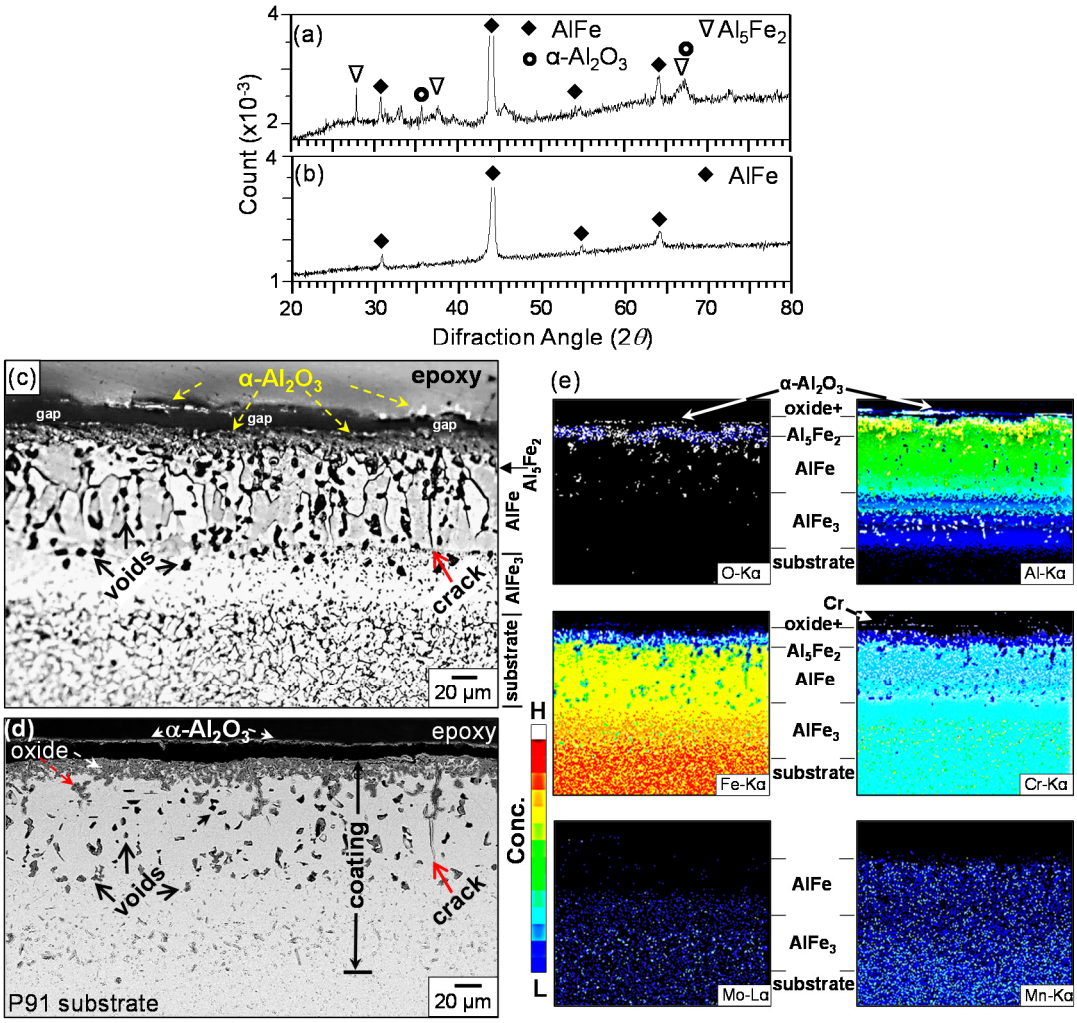

Figure 5. Al hot-dipped P91 steel after oxidation at 800 °C for 100 h. (**a**) XRD pattern before grinding; (**b**) XRD pattern after grinding off the surface; (**c**) cross-sectional optical microstructure (etched); (**d**) EPMA BSE cross-sectional image; (**e**) EPMA maps of (**d**).

The Vickers microhardness of the sample, outlined in Figures 2 and 5, is displayed in Figure 6. Before heating, the average microhardness of the Al-rich topcoat, $Al_{13}Fe_4$ layer, Al_5Fe_2 layer,

and substrate was 105, 863, 1031, and 228 Hv, respectively. The lowest and highest microhardness was similarly reported in the Al-topcoat and Al_5Fe_2-alloy layer, respectively [4,13]. The Al-rich topcoat disappeared after oxidation at 800 °C for 100 h in air [13]. Heating broadened and softened the alloy layer so that the average microhardness of the (oxides, Al-Fe)-mixed layer, AlFe layer, $AlFe_3$ transient layer, and the substrate became 879, 507, 336, and 227 Hv, respectively. The increment of the surface hardness of the hot-dip aluminized P91 steel improves the wear resistance and thereby the performance of structural components [13].

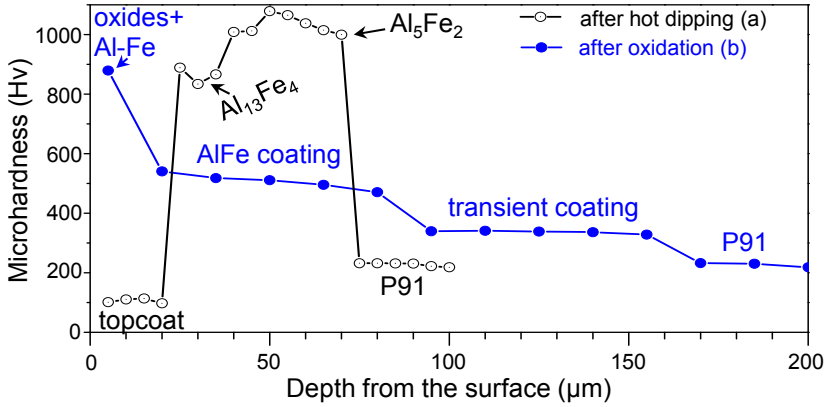

Figure 6. Vickers microhardness variation along the depth for Al-hot dipped P91 steel: (**a**) before oxidation; (**b**) after oxidation at 800 °C for 100 h.

Figure 7 shows the XRD/SEM/EDS/EPMA results of the Al hot-dipped P91 steel after oxidation at 900 °C for 20 h. In Figure 7a, α-Al_2O_3(m) and Fe_2O_3(w) formed on the $AlFe_3$(s) coating. From Figure 7b,c, it is seen that the ~35 μm-thick (α-Al_2O_3, Fe_2O_3)-mixed oxide layer either detached or adherent (spots 1–2), ~90 μm-thick $AlFe_3$ layer (spots 3–5), and the ~255 μm-thick Fe(Al) coating (spots 6–18; α-Fe layer dissolved with some Al) existed on the substrate (spots 19–22). Iron diffused outwardly to form Fe_2O_3 (Figure 7a), whose amount was smaller than that of α-Al_2O_3 (spots 1–2 in Figure 7c). Moving from the oxide layer through the $AlFe_3$/Fe(Al) coating to the substrate, the concentration of Al and oxygen decreased, while those of Fe and Cr increased (Figure 7c). In Figure 7b, a scratch was shown at the surface. It was made using a knife prior to oxidation in order to study the oxidation mechanism of the hot dipped sample. If the scratch was buried by oxides after oxidation, the oxidation had to be controlled by the outward diffusion of substrate elements. However, this was not observed in Figure 7b, indicating that no significant outward diffusion of substrate elements to form the oxide scale had occurred. In Figure 7d, internal oxides, voids, and cracks were seen in the $AlFe_3$/Fe(Al) coating. Voids in the $AlFe_3$ layer were coarser than those in the Fe(Al) layer, because the inward transport of Al from the $AlFe_3$ coating into the Fe(Al) coating occurred faster than the outward migration of substrate elements such as Fe, Cr, Mo, Mn, Si, and V towards the surface [6] (Figure 7e). The substrate was void-free (Figure 7d). Figure 7e indicates that substrate elements diffused up to the surface, while Al diffused inwardly down to the Fe(Al) layer. In Figure 5c, the ~4 μm-thick α-Al_2O_3 layer, ~20 μm-thick Al_5Fe_2-rich layer, ~70 μm-thick AlFe layer, and ~65 μm-thick transient $AlFe_3$ layer existed on the substrate. When compared to Figure 5c, the following observations were noticeable due to the enhanced reaction rate and counterdiffusion at 900 °C. The (Al_5Fe_2-rich layer)/(AlFe layer) (Figure 5c) changed to the $AlFe_3$ coating (Figure 7c). The transient $AlFe_3$ layer (Figure 5c) changed to the Fe(Al) coating (Figure 7c). Grains in the Fe(Al) coating were much more coarse, and columnar than those in the transient $AlFe_3$ layer, confirming the increased growth rate of grains along the direction of counterdiffusion (Figure 7b). The α-Al_2O_3-rich scale that had some Fe_2O_3 grew predominantly inwards through the cracks (Figure 6d,e). The densities of $Al_{13}Fe_4$, Al_5Fe_2, AlFe, and $AlFe_3$ were 3.849, 3.96, 5.67, and 6.57 g·cm^{-3}, respectively. When hard,

brittle $Al_{13}Fe_4$ and Al_5Fe_2 layers, viz. low density phases, transformed to soft, ductile AlFe and $AlFe_3$ layers, viz. high density phases, the volume shrank, and therefore cracks were generated [14,15].

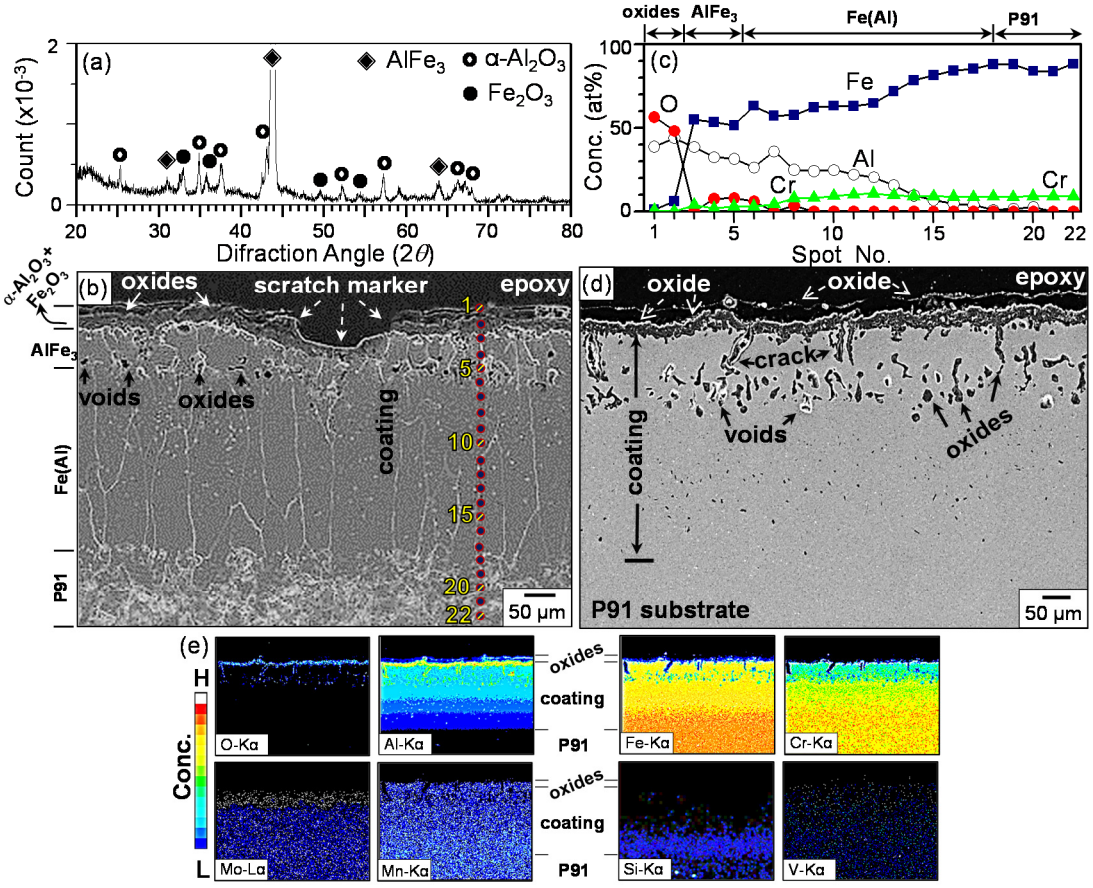

Figure 7. Al hot-dipped P91 steel after oxidation at 900 °C for 20 h: (**a**) XRD pattern; (**b**) cross-sectional SEM image (etched); (**c**) EDS concentration profiles along spots 1–22 marked in (**b**); (**d**) cross-sectional EPMA image (unetched); (**e**) EPMA maps of (**d**).

The beneficial effect of Al hot-dipping in increasing the oxidation resistance of P91 steel is clearly seen from the comparison of Figures 7 and 8. The uncoated P91 steel formed an outer 425 μm-thick oxide scale and an inner 360 μm-thick oxide scale (Figure 8a). Cracks and voids were generated due to the increased thermal and growth stresses aroused in the thick scale, which deteriorated the scale adherence. The outer scale consisted primarily of Fe_2O_3 (Figure 8b), where a small amount of alloying elements such as Cr, Mo, Mn, Si, and V dissolved (Figure 8c). All the matrix elements such as Fe, Cr, Mo, Mn, and Si were found in the inner scale (Figure 8c). In Figure 8d, white spots were Pd particles that were sprayed on the surface prior to oxidation in order to study the oxidation mechanism of P91 steel. The bottom of the Pd particles corresponded to the original sample surface. The Pd marker experiment indicated that the outer scale formed primarily by the outward diffusion of substrate elements, while the inner scale formed by the inward transport of oxygen. When cations diffused outwardly, they pushed the Pd particles upward, which was responsible for the Pd signal in the middle of the outer scale (Figure 8c) and the Pd particles above the interface of the outer/inner oxide scale (Figure 8d). In the case of coated steel, the selective oxidation of Al led to the formation of the Al_2O_3-rich scale, which effectively protected the steel from oxidation. The oxide scale partially broke and spalled owing to its mismatch in the thermal expansion coefficient with the underlying Al-Fe coating that underwent the phase transformation during oxidation.

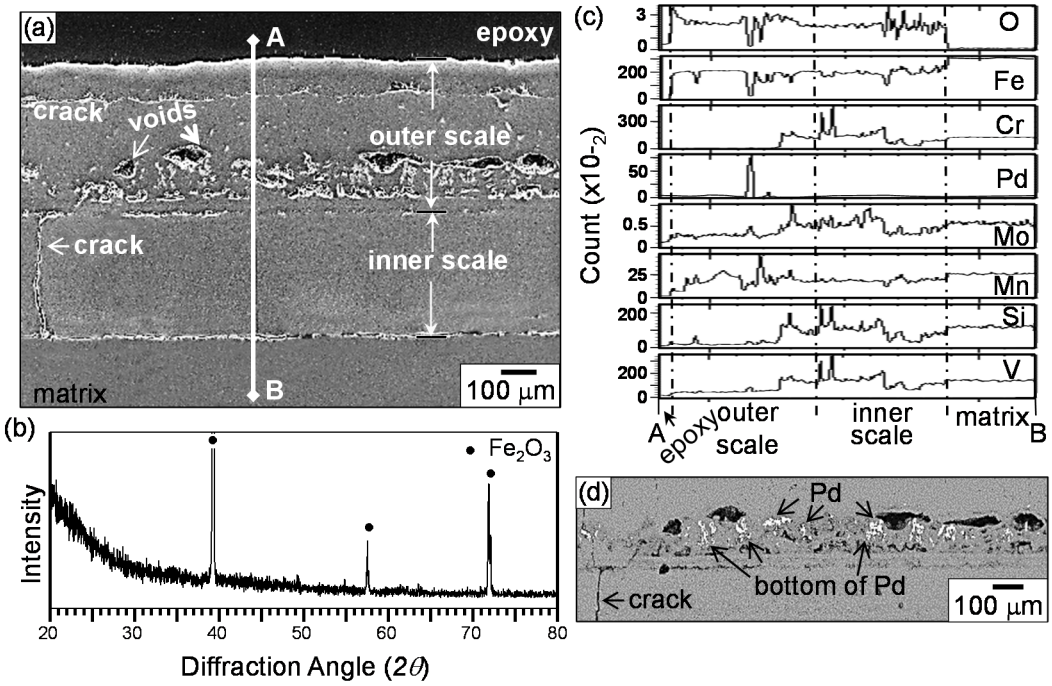

Figure 8. Uncoated P91 steel after oxidation at 900 °C for 20 h: (**a**) cross-sectional EPMA image (unetched); (**b**) XRD pattern; (**c**) EPMA line profiles along A–B marked in (**a**); (**d**) enlarged SEM-BSE image around the outer/inner oxide scale shown in (**a**).

4. Conclusions

The Al hot-dipped coating that formed on P91 steel consisted of the topcoat (rich in Al, with a small amount of needle-like Al_5Fe_2 and $Al_{13}Fe_4$) and alloy layer (marginally consisted of $Al_{13}Fe_4$, and mostly consisted of Al_5Fe_2, with tiny scattered Al_9Cr_4 precipitates). Interdiffusion between the Al and substrate elements during oxidation always broadened the coating, diluted the concentration of Al to change the composition of the Al-Fe phases, and mechanically softened the coating through counterdiffusion. The oxidation at 700 °C for 100 h led to the formation of the poorly adherent α-Al_2O_3 scale, changed the Al-rich topcoat to the $Al_{13}Fe_4$-rich layer containing some Al_5Fe_2, and also changed the alloy layer that consisted of ($Al_{13}Fe_4$ layer/Al_5Fe_2 layer) to the Al_5Fe_2 layer having fine, elongated grains, below which another thin AlFe layer was newly formed at the coating/substrate interface. The oxidation at 800 °C for 100 h similarly formed the poorly adherent α-Al_2O_3 scale. Since counterdiffusion progressed further, the $Al_{13}Fe_4$-rich layer containing some Al_5Fe_2 changed to the AlFe-rich layer containing some Al_5Fe_2, changed the Al_5Fe_2 layer having fine, elongated grains to the AlFe layer having coarse, columnar grains, and formed the wide $AlFe_3$ layer instead of the thin AlFe layer on the substrate. When oxidized further at 900 °C for 20 h, the increased counterdiffusion and reaction rate eventually led to the formation of the (α-Al_2O_3, Fe_2O_3)-mixed oxide scale because Al was diluted and Fe was accumulated at the surface, whilst the coating consisted of the outer $AlFe_3$ layer and the inner Fe(Al) layer. The results indicated that hot-dip aluminizing increased the high-temperature oxidation resistance of P91 steel because of the formation of poorly adherent α-Al_2O_3 surface scale and AlFe/$AlFe_3$ alloy layer phases, regardless of the cracks and voids, which were unavoidable in the coating during oxidation. The uncoated P91 steel failed to provide the oxidation resistance and formed the thick oxide scales that had cracks and voids.

Acknowledgments: This work was supported under the framework of the international cooperation program managed by the National Research Foundation of Korea (2016K2A9A1A01952060).

Author Contributions: Muhammad Ali Abro conceived of and carried out the experimental tests, and wrote the paper; Dong Bok Lee reviewed the data, revised, and finalized the paper.

Conflicts of Interest: The authors have no conflict of interest.

References

1. Vossen, J.P.T.; Gawenda, P.; Rahts, K.; Röhrig, M.; Schorr, M.; Schütze, M. Limits of the oxidation resistance of several heat-resistant steels under isothermal and cyclic oxidation as well as under creep in air at 650 °C. *Mater. High Temp.* **1997**, *14*, 387–401. [CrossRef]
2. Wright, I.G.; Dooley, R.B. A review of the oxidation behaviour of structural alloys in steam. *Int. Mater. Rev.* **2010**, *55*, 129–167. [CrossRef]
3. Sundararajan, T.; Kuroda, S.; Seal, S. High temperature corrosion of nanoceria coated 9Cr-1Mo ferritic steel in air and steam. *Surf. Coat. Technol.* **2006**, *201*, 2124–2130. [CrossRef]
4. Kobayashi, S.; Yakou, T. Control of intermetallic compound layers at interface between steel and aluminum by diffusion-treatment. *Mater. Sci. Eng. A* **2002**, *338*, 44–53. [CrossRef]
5. Abro, M.A.; Bak, S.H.; Lee, D.B. High temperature corrosion of Al-1% Si coated carbon steels in N_2/0.1% H_2S Gas. *J. Nanosci. Nanotechnol.* **2016**, *16*, 11247–11251. [CrossRef]
6. Wang, C.J.; Chen, S.M. The high-temperature oxidation behavior of hot-dipping Al–Si coating on low carbon steel. *Surf. Coat. Technol.* **2006**, *200*, 6601–6605. [CrossRef]
7. Abro, M.A.; Lee, D.B. Effect of Al hot-dipping on high-temperature corrosion of carbon steel in N_2/0.1% H_2S gas. *Metals* **2016**, *6*, 38. [CrossRef]
8. Richards, R.W.; Jones, R.D.; Clements, P.D.; Clarke, H. Metallurgy of continuous hot dip aluminizing. *Int. Mater. Rev.* **1994**, *39*, 191–212. [CrossRef]
9. Abro, M.A.; Lee, D.B. High temperature corrosion of hot-dip aluminized steel in Ar/1%SO_2 gas. *Met. Mater. Int.* **2017**, *23*, 92–97. [CrossRef]
10. Bouche, K.; Barbier, F.; Coulet, A. Intermetallic compound layer growth between solid iron and molten aluminium. *Mater. Sci. Eng. A* **1998**, *249*, 167–175. [CrossRef]
11. EI-Mahallawy, N.A.; Taha, M.A.; Shady, M.A.; EI-Sissi, A.R.; Attia, A.N.; Reif, W. Analysis of coating layer formed on steel strips during aluminising by hot dipping in Al-Si baths. *Mater. Sci. Technol.* **1997**, *13*, 832–840. [CrossRef]
12. Abro, M.A.; Lee, D.B. Aluminizing and corrosion of carbon steels in N_2/0.5% H_2S Gas at 650–850 °C. *J. Kor. Inst. Surf. Eng.* **2015**, *48*, 110–114. [CrossRef]
13. Deqing, W. Phase evolution of an aluminized steel by oxidation treatment. *Appl. Surf. Sci.* **2008**, *254*, 3026–3032. [CrossRef]
14. Cheng, W.J.; Chang, Y.Y.; Wang, C.J. Observation of high-temperature phase transformation in the aluminide Cr-Mo steel using EBSD. *Surf. Coat. Technol.* **2008**, *203*, 401–406. [CrossRef]
15. Chang, Y.Y.; Tsaur, C.C.; Rock, J.C. Microstructure studies of an aluminide coating on 9Cr-1Mo steel during high temperature oxidation. *Surf. Coat. Technol.* **2006**, *200*, 6588–6593. [CrossRef]
16. Cheng, W.J.; Wang, C.J. EBSD characterization of high-temperature phase transformations in an Al-Si coating on Cr-Mo steel. *Mater. Charact.* **2012**, *64*, 15–20. [CrossRef]
17. Chang, Y.Y.; Cheng, W.J.; Wang, C.J. Growth and surface morphology of hot-dip Al-Si on 9Cr-1Mo steel. *Mater. Charact.* **2009**, *60*, 144–149. [CrossRef]
18. Wang, D.; Shi, Z.; Zou, L. A liquid aluminum corrosion resistance surface on steel substrate. *Appl. Surf. Sci.* **2003**, *214*, 304–311.
19. Palm, M. The Al-Cr-Fe system-Phases and phase equilibria in the Al-rich corner. *J. Alloys Compd.* **1997**, *252*, 192–200. [CrossRef]
20. Titran, R.H.; Vedula, K.M.; Anderson, G.G. High temperature properties of equialomic FeAl with ternary additions. *Mater. Res. Soc. Symp. Proc.* **1985**, *39*, 309–317. [CrossRef]